Paths to globally generalized synchronization in scale-free networks

Yao-Chen Hung*
Institute of Physics, Academia Sinica, Nankang, Taipei 11529, Taiwan

Yu-Ting Huang and Ming-Chung Ho
Nonlinear Science Group, Department of Physics, National Kaohsiung Normal University, Kaohsiung 824, Taiwan

Chin-Kun Hu†
Institute of Physics, Academia Sinica, Nankang, Taipei 11529, Taiwan
and Center for Nonlinear and Complex Systems and Department of Physics, Chung Yuan Christian University, Chungli 32023, Taiwan

(Received 23 August 2007; revised manuscript received 3 December 2007; published 16 January 2008)

We apply the auxiliary-system approach to study paths to globally generalized synchronization in scale-free networks of identical chaotic oscillators, including Hénon maps, logistic maps, and Lorentz oscillators. As the coupling strength ε between nodes of the network is increased, transitions from partially to globally generalized synchronization and intermittent behaviors near the synchronization thresholds, are found. The generalized synchronization starts from the hubs of the network and then spreads throughout the whole network with the increase of ε. Our result is useful for understanding the synchronization process in complex networks.

DOI: 10.1103/PhysRevE.77.016202 PACS number(s): 05.45.Xt, 89.75.Fb, 89.75.Hc

I. INTRODUCTION

Synchronization has attracted much attention in recent decades [1] and appears in a wide variety of mathematical (such as coupled map models on lattices [2], stochastic Kuramoto model [3]), physical (such as laser [4], Josephson junction arrays [5], quantum systems [6]), physiological [7], biological [8], ecological [9], chemical [10], and financial systems [11]. From the relationship among the components of the system, synchronization can be classified into several different categories. In complete synchronization (CS), the interacting components adjust their states so that they evolve on an identical trajectory [12]. In the phase synchronization (PS), there exists some relations between the phases of interacting components, while the amplitudes still remain irregular and, in general, uncorrelated [13]. Generalized synchronization (GS) represents another degree of coherence, i.e., the emergence of some functional relation between the states of interacting components [14]. Depending on different coupling methods and coupling strengths, other types of synchronization can also be observed; for instance, lag synchronization [15], anticipation synchronization [16], reduce-order synchronization [17], and so on. These various degrees of synchronization have been recognized as different expressions of a universal conception [18].

Although synchronization has been intensively studied, the synchronization in complex networks still contains some open and crucial questions [19]. Such a subject is to explore how the collective behaviors in complex networks are influenced by the complex topological structures [20]. The study is important because in the real world, many networks sustain dynamical process, and the interactions among elements define the connections in the networks [21,22]. The emergence of clustering or partial synchronization, where some of the subsystems synchronize and the others do not, is another peculiar feature represented in complex networks [23–25]. A good understanding of the transitions from turbulent, partial synchronization, to global synchronization would be beneficial to realize the self-organization phenomena in nature [25,26], and give possible implications for neuroscience, such as epilepsy [27]; notwithstanding the inherent interest in the problem itself.

In this paper, we consider synchronization in scale-free networks (SFN) [22,25] consisting of symmetrically (bidirectionally) coupled chaotic oscillators. Although CS and PS have been observed and well studied in SFN [25,28], to our knowledge, other levels of synchrony are still not detected or well studied. Here we apply the auxiliary-system approach [29,30], to find GS in SFN, including the transitions from partial GS (PGS) to global GS (GGS). Our investigation reveals some dynamical importance. Besides a few specified coupling strategies, CS is typically regarded as the form of synchronization in coupled identical systems, while GS is expected to be in coupled nonidentical systems [31]. However, the present work shows that GS appears in a network of identical oscillators. Actually, the nonidentity among all components is resulted from the heterogeneity in degree (connectivity) which induces the distinct chaotic behaviors of local mean fields. Numerical experiments show that the nodes do not achieve GS simultaneously. In general, GS starts from some hubs with highly connected nodes, then spreads over the whole network from the nodes connecting to hubs. Such results not only give us an insight into the synchronization process but also provide a perspective to understand the role of topological hubs in dynamic behavior of synchronization in complex networks.

This paper is organized as follows. In Sec. II, we review the transitions from partial GS to global GS in two mutually (bidirectionally) coupled Hénon maps [32] with different parameters. Instead of using the continuous oscillators [30], we have demonstrated that discrete maps with bidirectional cou-

*ychung@phys.sinica.edu.tw
†huck@phys.sinica.edu.tw

plings can also reveal the cascade transitions. Two types of dynamical behaviors called intermittent partial GS (IPGS) and intermittent global GS (IGGS) are detected in the vicinity of threshold coupling. The intermittent behaviors near the synchronization thresholds are demonstrated to be the typical on-off intermittency obeying a $-3/2$ power law. In Sec. III, the present idea is extended to SFN of chaotic systems. Hénon maps, logistic maps, and Lorenz oscillators are adopted as the local dynamics in our working models. We present the results of the route toward global synchronization and find that the scenario is intrinsically connected with the topology of interactions. In Sec. IV, we discuss our results.

II. TWO MUTUALLY COUPLED NONIDENTICAL MAPS

Consider two mutually (bidirectionally) coupled Hénon maps [32] with different parameters. The formulations governing the evolution of the coupled subsystems are given by

$$x_1(t+1) = 1.4 - [\varepsilon x_1(t)x_2(t) + (1-\varepsilon)x_1^2(t)] + b_1 y_1(t),$$

$$y_1(t+1) = x_1(t), \tag{1}$$

$$x_2(t+1) = 1.4 - [\varepsilon x_2(t)x_1(t) + (1-\varepsilon)x_2^2(t)] + b_2 y_2(t),$$

$$y_2(t+1) = x_2(t). \tag{2}$$

Here $(x_1(t), y_1(t))^T \equiv \mathbf{v}_1(t)$ and $(x_2(t), y_2(t))^T \equiv \mathbf{v}_2(t)$ are the vector states of the two subsystems, and $\varepsilon \in [0,1]$ denotes the coupling strength. Constants b_1 and b_2 are the chaotic parameter of the Hénon map, and here we choose $b_1=0.1$ and $b_2=0.3$ to ensure the typical chaotic behaviors. The coupling is diffusive.

We will use the auxiliary-system approach [29] to detect the nonlinear correlations between two coupled systems. In addition to the drive-response systems, the method has been demonstrated to be available for mutually coupled elements [30]. The method starts from creating two replicas of the original subsystems. The vector states of the replicas $\mathbf{v}_{1'}(t) \equiv (x_{1'}(t), y_{1'}(t))^T$ and $\mathbf{v}_{2'}(t) \equiv (x_{2'}(t), y_{2'}(t))^T$ obey, respectively, the equations

$$x_{1'}(t+1) = 1.4 - [\varepsilon x_{1'}(t)x_2(t) + (1-\varepsilon)x_{1'}^2(t)] + b_1 y_{1'}(t),$$

$$y_{1'}(t+1) = x_{1'}(t), \tag{3}$$

$$x_{2'}(t+1) = 1.4 - [\varepsilon x_{2'}(t)x_1(t) + (1-\varepsilon)x_{2'}^2(t)] + b_2 y_{2'}(t),$$

$$y_{2'}(t+1) = x_{2'}(t). \tag{4}$$

Equations (1)–(4) show that subsystems $1'$ and 1 are driven by 2, while $2'$ and 2 are driven by 1, but they evolve from different initial conditions, $\mathbf{v}_{1,2}(t_0) \neq \mathbf{v}_{1',2'}(t_0)$. The core of such a method is the following: If the GS relation $H_{1\to 2}$ is constructed and unique, the phase trajectories of subsystems $2'$ and 2 would coincide after the transient dies out, where $H_{1\to 2}$ denotes a functional relationship $\mathbf{v}_2(t) = \mathbf{H}_{1\to 2}[\mathbf{v}_1(t)]$.

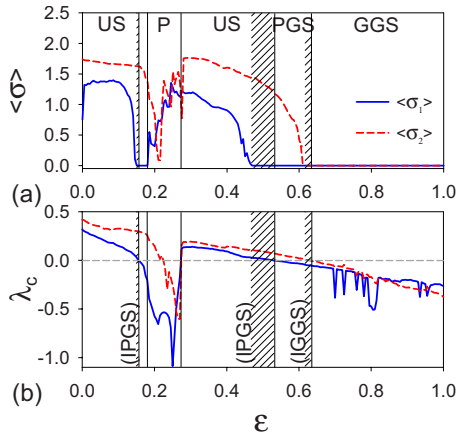

FIG. 1. (Color online) (a) The average synchronization errors $\langle\sigma\rangle$ and (b) the MCLE λ_c of two mutually coupled Hénon maps with $b_1=0.1$ (solid lines) and $b_2=0.3$ (dashed lines). The symbols US, P, PGS, GGS, IPGS, and IGGS, respectively, correspond to unsynchronized state, periodic state, partial GS, global GS, intermittent partial GS, and intermittent global GS. The area $\varepsilon \in [0.16, 0.18]$ corresponds to another PGS state.

Analogously, the construction of the GS relation $H_{2\to 1}$ ($\mathbf{v}_1(t) = \mathbf{H}_{2\to 1}[\mathbf{v}_2(t)]$) would result in the coincidence of trajectories of subsystems $1'$ and 1. The auxiliary method thus provides a much simpler criterion to measure the presence of GS.

There is an interesting question: Do subsystems $1'$-1 and $2'$-2 become completely synchronized simultaneously? Or in other words, are the GS relations $H_{1\to 2}$ and $H_{2\to 1}$ built at the same coupling threshold? To explore such a problem, we calculate the average synchronization error $\langle\sigma_{1,2}\rangle = (1/T)\Sigma_{t=1}^{T}|\mathbf{v}_{1,2}(t) - \mathbf{v}_{1',2'}(t)|$ as a function of ε, as shown in Fig. 1(a). The figure is obtained by discarding long transients ($\sim 10^6$) and averaging over 100 different realizations with random initial conditions. We also have a sufficiently large value of T. In Fig. 1(a), the symbols US, P, PGS, and GGS correspond to the unsynchronized state, periodic state, partial generalized synchronization, and global generalized synchronization, respectively. When the coupling strength is extremely weak, both $\langle\sigma_1\rangle$ and $\langle\sigma_2\rangle$ are nonzero and it indicates that two systems evolve independently and remain as the US state. For $\varepsilon \in [0.16, 0.18]$, the situation $\langle\sigma_1\rangle = 0$ and $\langle\sigma_2\rangle \neq 0$ indicates the establishment of the formation $H_{2\to 1}$ and the absence of the reverse relation $H_{1\to 2}$. Such an asymmetric synchrony is recognized as the PGS. Afterward, for $\varepsilon \in [0.185, 0.275]$, the evolutions of subsystems are suppressed and display the periodic motions, which can be confirmed by the negative global Lyapunov exponents (not presented) [33]. In this region, the global dynamics of two coupled maps depending on initial conditions and coupling strength presents synchronization behaviors or unsynchronized iterations with phase slips. The above results show that the transitions of the route, from PGS to GGS, are typical but not unique. Other transitions, for example, PGS to P in our case, is also possible. After $\varepsilon > 0.275$, two coupled Hénon maps undergo the generic cascade from US, PGS to GGS with the increase of coupling strength. Here GGS indicates

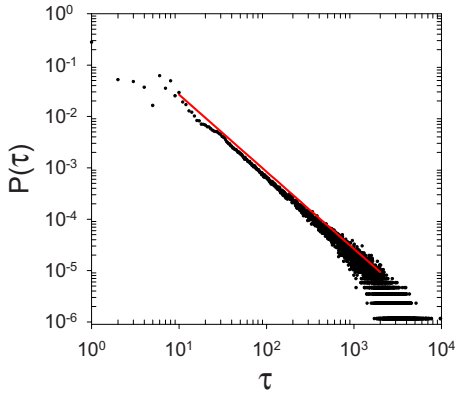

FIG. 2. (Color online) The statistical distribution of laminar phases in the IPGS region ($\varepsilon=0.52$). The slope of the reference line [gray (red)] is $-3/2$.

both relations $H_{1\to2}$ and $H_{2\to1}$ are well established.

The maximum conditional Lyapunov exponent (MCLE) λ_c is another parameter to detect GS [31]. The negative value of λ_c ensures the achievement of GS for a subsystem. Figure 1(b) shows the MCLE λ_c against ε and gives a similar picture to describe the route from US to GGS. However, as we can observe, the synchronized thresholds between Fig. 1(a) and Fig. 1(b) are visibly different. More clearly, the synchronization condition $\langle\sigma\rangle=0$ is achieved while λ_c still remains positive, as presented by meshed regions. Such a phenomenon is called the spurious synchronization (SS), which is arisen from the finite precision in numerical simulations [34]. SS occurs when the system possesses a large contracting region, especially for the discrete map [35].

The coexistence of contracting and diverging regions not only induces the artificial synchrony but also results in the intermittent behaviors in the vicinity of the synchronization threshold [36]. In our case, at $\varepsilon=0.52$ the evolution of $\sigma_1(t)$ presents intermittent deviations from the synchronized state (not presented). In other words, the GS relationship $H_{2\to1}$ conserves most of the time, but it would be interrupted by breaking of the functional relation during some time intervals. No matter if $H_{2\to1}$ exists or not, the reverse relation $H_{1\to2}$ is absent at such a coupling strength. We define this asymmetrically intermittent relation as the intermittent PGS (IPGS), which is analogous with the intermittent GS (IGS) reported previously [37]. Furthermore, near the transition to GGS, $H_{2\to1}$ holds robustly while $H_{1\to2}$ remains unstable. We define the phenomenon as the intermittent GGS, analogously.

The intermittent behavior of the synchronization error is reminiscent of the on-off intermittency. To characterize the statistical property of IPGS and IGGS, we analyze the histogram distribution of laminar phases length τ. The criterion $\sigma(t)\leq10^{-2}$ is given to define the laminar phases or the off states, and $\sigma(t)>10^{-2}$ corresponds to the on states. We collect the laminar phases until the SS is achieved, and perform the collection repeatedly with different initial conditions. The statistical distribution of laminar phases of $\sigma_1(t)$ at $\varepsilon=0.52$ is shown in Fig. 2. The linearity of the logarithm-logarithm plot suggests that the distribution obeys a power law with a universal exponent $-3/2$ [34]. Such a $-3/2$ law does not sensitively depend on the choice of laminar phases criterion, and it holds within the IPGS and IGGS areas. Therefore, both IPGS and IGGS appear to be the on-off intermittency.

III. COUPLED IDENTICAL MAPS ON THE SCALE-FREE NETWORKS

In this section, we extend the previous idea to a heterogeneously complex network. Consider a network consisting of N nodes with the scale-free topology [22]. Each node stands for a dynamical system, and links in the network represent the interactions (or couplings) between nodes. First we choose the Hénon map [32] as the local dynamics, and the coupled maps network reads as

$$x_i(t+1)=1.4-[\varepsilon x_i(t)X_i(t)+(1-\varepsilon)x_i^2(t)]+b_iy_i(t),$$

$$y_i(t+1)=x_i(t), \tag{5}$$

where the subscript $i=1,2,\ldots,N$ denotes the node index, and the chaotic parameter $b_i=0.1$, $\forall\ i$. $X_i(t)\equiv(1/k_i)\Sigma_{j=1}^{N}C_{ij}x_j(t)$ denotes the local mean field of the node i, where C_{ij} is an element of the $N\times N$ adjacency matrix C that characterizes the topology of such a network. Elements C_{ij} take the value 1 when there is a connection between nodes i and j with $i\neq j$ and 0 otherwise ($C_{ii}=0$). The connections are bidirectional; i.e., $C_{ij}=C_{ji}$ and C is a symmetric matrix. $k_i=\Sigma_jC_{ij}$ is the degree of node i.

The adjacency matrix C is generated by using the Barabási-Albert scale-free model [22]. Starting with a small number m_0 of fully interconnected nodes, a new node is introduced to connect with m ($m\leq m_0$) previous node at every time step. The connection probability depends on the degree of already-existing nodes (preferential attachment). After l time steps, the above algorithm creates a network with $N=l+m_0$ nodes. As a general feature, the connectivity distribution follows a power law with an exponent constant $\lambda\approx3$, regardless of m_0 and m. To shed light on the relation between underlying topology of interactions and synchronization processes, we concentrate on the network with a small number of connections, the network with tree structure ($m_0=m=1$), throughout this paper. In such a sparsely connected network, the fully CS state, i.e., all the trajectories of Hénon maps coincide with each other, is unrealizable for all values of ε [28]. Consequently, we focus on the weaker expression of synchronization, the GS behaviors. The effect of a larger m will be discussed later.

To investigate GS behaviors in a scale-free dynamical network, we follow the idea of Sec. II to propose an auxiliary system consisting of replicate nodes. The schematic description is illustrated in Fig. 3, where a replica and its correspondingly original node share an identical formulation and a common local mean field. The evolution of the auxiliary system is then written as

$$x_{i'}(t+1)=1.4-[\varepsilon x_{i'}(t)X_i(t)+(1-\varepsilon)x_{i'}^2(t)]+b_iy_{i'}(t),$$

$$y_{i'}(t+1)=x_{i'}(t). \tag{6}$$

The vector state of node i, $(x_i(t),y_i(t))^T\equiv\mathbf{v}_i(t)$, and the replica $(x_{i'}(t),y_{i'}(t))^T\equiv\mathbf{v}_{i'}(t)$ evolve from different initial states

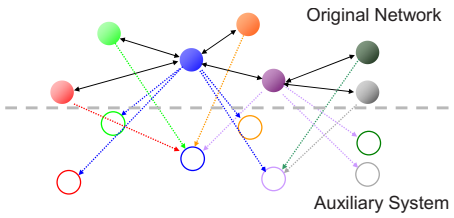

FIG. 3. (Color online) A schematic description of the auxiliary-system approach to study the GS phenomena in a scale-free dynamical network. An auxiliary node (empty circle) and its correspondingly original one (solid circle) are drawn by the same color. The arrows indicate the coupling directions.

which lie in the same basin of the attractor. By analogy with previous statements, the coincidence of $\mathbf{v}_i(t)$ and $\mathbf{v}_{i'}(t)$ indicates the achievement of GS for the node i.

Now we look into the synchronization phenomena of the network. The network size $N=50$ and an invariant coupling configuration (will be represented later) are chosen throughout the paper. We calculate the average synchronization error $\langle\sigma_i\rangle=(1/T)\Sigma_{t=1}^{T}|\mathbf{v}_i(t)-\mathbf{v}_{i'}(t)|$ as a function of the coupling strength ε over 100 realizations with random initial conditions and a long transition T. Figure 4(a) presents our numerical results for three different nodes $i=2,22,48$ with degrees $k_2=9$, $k_{22}=3$, and $k_{48}=1$, respectively. The network presents various collective behaviors against different ε.

When interactions between nodes are weak, the ensemble is dominated by the US state. In the region $\varepsilon\in[0.135,0.210]$, where nodes show a variety of local dynamical behaviors, namely period, quasiperiodic, and even chaotic motions, depending sensitively on the initial conditions. Such a region is defined as the varied state (V). If ε is further increased, one may find a discrete series for $\langle\sigma_i\rangle$ becoming zero at different ε. As referred to above, the CS relation between the node i and its replica ($\langle\sigma_i\rangle=0$) indicates the emergence of the GS relationship between the node i and

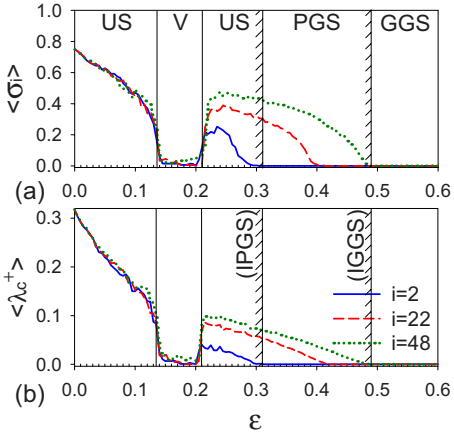

FIG. 4. (Color online) (a) Average synchronization errors and (b) average positive MCLE of the coupled Hénon maps network for nodes $i=2,22,48$ with degrees $k_2=9$, $k_{22}=3$, and $k_{48}=1$. The symbols US, V, PGS, GGS, IPGS, and IGGS, respectively, correspond to unsynchronized state, varied state, partial GS, global GS, intermittent partial GS, and intermittent global GS.

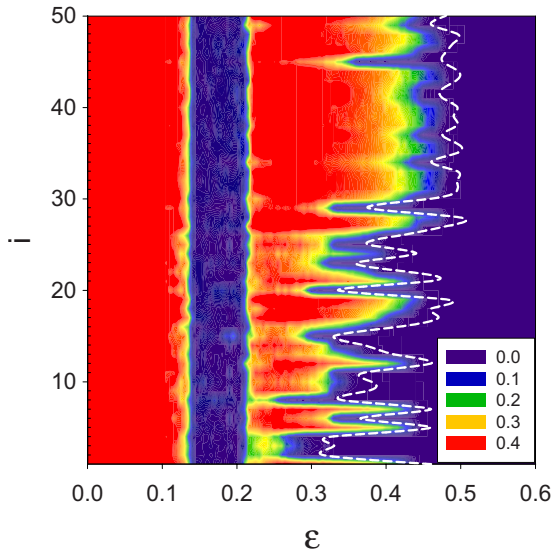

FIG. 5. (Color online) The diagram shows the average synchronization errors $\langle\sigma_i\rangle$ between the coupled Hénon maps network and its replica as a function of coupling strength ε for $1\leq i\leq 50$, where the notation i denotes the node index. The color spectrum represents different values of $\langle\sigma\rangle$. The exact synchronization thresholds determined by $\langle\lambda_c^+\rangle$ are labeled by a dashed line.

its corresponding local mean field X_i. In our case, the node $i=2$ is the first one being synchronized, and the node $i=48$ is one of the latest nodes being entrained in terms of ascending ε, as shown in Fig. 5. Between the two extremes, some nodes are entrained while the others are not, which defines the partial GS state. Furthermore, when all the values of $\langle\sigma_i\rangle$ converging to zero indicates that the functional relations between the nodes and their corresponding X_i are globally established. In other words, the GGS state is achieved. With the increase of ε, Fig. 5 clearly shows the scenario from US, PGS, to GGS in our working network. The high dependence of critical coupling strengths upon the values of degree and the topologically relative positions would be unveiled later.

The synchronization thresholds need to be confirmed further by using MCLE. Due to the dependence of individual dynamics on initial conditions, the average positive MCLE $\langle\lambda_c^+\rangle$ is calculated to determine the exact synchronization thresholds [38]. The definition is given by

$$\langle\lambda_c^+\rangle=\frac{1}{M}\sum_{j=1}^{\lambda_c>0}\lambda_c(j), \tag{7}$$

where $\lambda_c(j)$ denotes the MCLE of the jth realization and $M=100$ is the amount of realizations with different initial conditions. Figure 4(b) illustrates the numerical results for $i=2$, 22, and 48, where the condition $\langle\lambda_c^+\rangle=0$ ensures the achievement of GS for a node. The synchronization thresholds determined by $\langle\sigma\rangle$ and $\langle\lambda_c^+\rangle$ present a slight mismatch, as aforementioned, which unveils the SS phenomenon existing in the coupled maps network. Near the synchronization threshold, each node also displays the typical intermittent GS behavior, i.e., the evolution of $\sigma_i(t)$ irregularly shows bursts

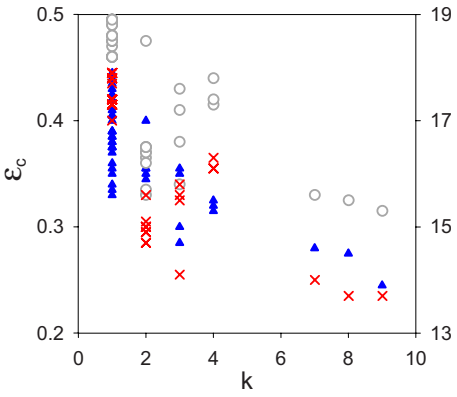

FIG. 6. (Color online) The values of synchronization threshold ε_c are shown as functions of the degree of nodes. Symbols represent the results of the network consisting of different dynamics, i.e., Hénon maps (circles), logistic maps (crosses), and Lorentz oscillators (triangles). The left-hand tick marks label the threshold values for Hénon maps and logistic maps, while the right-hand tick marks are for Lorentz oscillators.

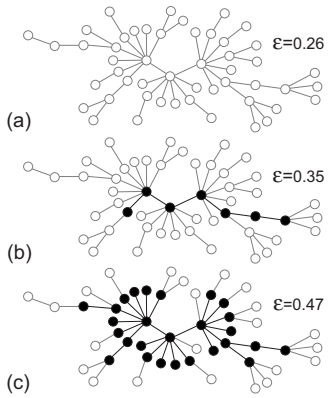

FIG. 7. Typical path to GGS in a scale-free network with nodes and coupling between nodes shown as empty circles and gray lines, respectively. There are $N=50$ nodes in this network and the hub has degree $k=8$. The entrained nodes are denoted by black circles, and the connections between them are replaced by black lines. As one can see, the GS starts from some central hubs, and then spreads throughout the network with the increase of ε.

deviating from the roughly synchronized state. Simultaneously, the histogram distribution of time intervals between two sequent bursts emerges a $-3/2$ power law, being identical to the one in the two coupled maps case. In other words, the dynamics represents the typical on-off intermittency.

The synchronization thresholds, determined by average positive MCLEs, of all nodes are represented in Fig. 5 by a dashed line. Note that for any two connected nodes, they are not entrained simultaneously regardless of the bidirectional couplings. The nonidentity of synchronization thresholds results from the heterogeneity in degree which induces the distinct chaoticity of local mean fields of all nodes. In particular, the highest connected nodes (hubs) are more easily entrained than the others with sparse connections, as depicted in Fig. 6 (circles). However, as one can observe in Fig. 6, the dependence of ε_c on k is both nonmonotonic and nonuniversal. To explain the reason for this phenomena, we investigate the impact of the topological property on the synchronization process and plot the evolution of dynamics toward GGS in Fig. 7. The underlying topology of the network used throughout this paper is drawn by empty circles (nodes) and gray lines (interactions). The nodes having achieved the GS are denoted by black circles, and the connections between them are replaced by black lines. From top to bottom, the three diagrams show different synchronization patterns in terms of ascending ε. For a complex network with heterogeneous connectivity, those units with much larger degree are entrained first and then, in a sequential process of increasing ε, assimilate the nodes connected to them. In other words, the GS starts at some central hubs and spreads from them, finally throughout the whole network. Our results not only confirm that hubs play the leading and essential roles in self-organizing toward global synchronization, but also generalize the conceptions in [39], where periodic oscillators and CS clustering behaviors are concentrated.

The aforementioned transition scenario persists in the networks with other sizes (the largest size we have investigated is $N=1000$) and different realizations of the adjacency matrix C. Besides concentrating on the scale-free network with tree topology ($m=1$), we have studied the effect of the larger m. For $m>1$, as a result of more compactly topological structure, the individuals achieve GS at smaller coupling strengths. Moreover, the variances of synchronization thresholds of nodes have diminished for a larger m ($m\geq 3$). That is to say, when the network becomes more compact, the nodes are entrained almost at the same ε, and the region representing the PGS behavior withers accordingly. Finally, after $m\geq 7$, the coupled maps show fully CS when ε exceeds a corresponding threshold [in our case, $\varepsilon_c(m=7)\sim 0.92$].

The route from PGS to GGS can also be observed in tree-type networks consisting of other chaotic elements, ranging from discrete maps to continuous oscillators, with different types of coupling functions. For example, a coupled one-dimensional map network is given by

$$x_i(t+1) = (1-\varepsilon)f(x_i(t)) + \varepsilon F_i(t), \tag{8}$$

where node index $i=1,2,\ldots,N$. The coupling term $F_i(t) \equiv (1/k_i)\Sigma_{j=1}^{N} C_{ij} f(x_j(t))$ is the local mean field of node i and the adjacency matrix C shares an identical topology with the network drawn in Fig. 7(a). The function $f(x(t))$ which governs the local dynamics is chosen as the well-known logistic map

$$f(x(t)) = \mu x(t)[1-x(t)], \tag{9}$$

where $\mu=4$ ensures all elements representing typical chaotic behaviors. The auxiliary model to unveil GS behavior in a coupled logistic maps network then is formulated as

$$x_{i'}(t+1) = (1-\varepsilon)f(x_{i'}(t)) + \varepsilon F_i(t). \tag{10}$$

The two networks evolve from different beginnings, i.e., $x_i(t_0) \neq x_{i'}(t_0)$, $\forall\ i$. The synchronization errors between the maps and their auxiliary partners are calculated and plotted against the coupling strength in Fig. 8. The dashed line marks the boundary between the unsynchronized state and the GS state of each node. In this diagram, one finds a clear

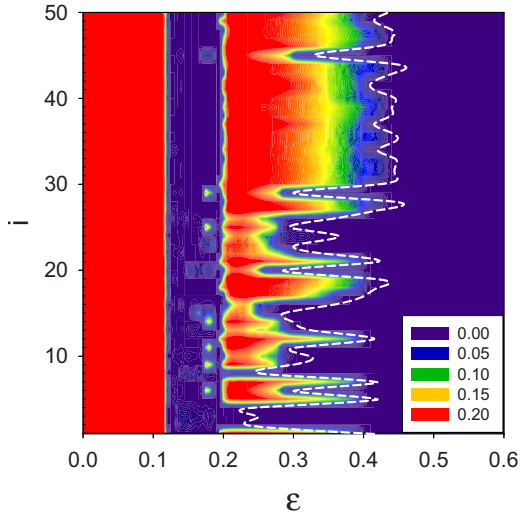

FIG. 8. (Color online) Average synchronization errors $\langle \sigma_i \rangle$ between the coupled logistic maps network and its replica vs ε for $1 \leq i \leq 50$. Notations follow Fig. 5.

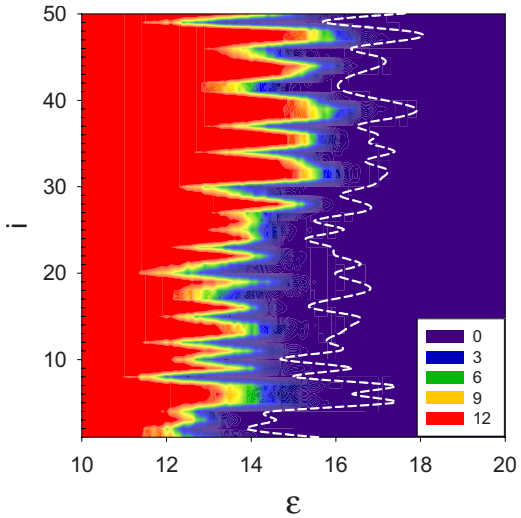

FIG. 9. (Color online) Average synchronization errors $\langle \sigma_i \rangle$ between the coupled Lorenz oscillators network and its replica vs ε for $1 \leq i \leq 50$. Notations follow Fig. 5.

cascade of transitions from disorder to partial and then global order by increasing the interacting strength. The crosses in Fig. 6 depict synchronization thresholds ε_c as functions of the degree of nodes. The intrinsic order toward self-synchronization, which is similar to Fig. 7, reveals high dependence upon the geometrical properties, i.e., the degree and the spatial location of nodes on the network.

Finally, we study the network of continuous chaotic oscillators. The mutually coupled Lorenz oscillators [40] on a scale-free network reads as

$$\dot{x}_i = \sigma(y_i - x_i) + \varepsilon(G_i - x_i),$$

$$\dot{y}_i = r x_i - y_i - x_i z_i,$$

$$\dot{z}_i = -b z_i + x_i y_i, \tag{11}$$

in which $i = 1, 2, \ldots, N$, $\sigma = 10$, $b = 8/3$, $r = 50$, and $G_i \equiv (1/k_i)\Sigma_{j=1}^{N} C_{ij} x_j$ is the local mean field of the ith node. Analogically, its auxiliary model is given by

$$\dot{x}_{i'} = \sigma(y_{i'} - x_{i'}) + \varepsilon(G_i - x_{i'}),$$

$$\dot{y}_{i'} = r x_{i'} - y_{i'} - x_{i'} z_{i'},$$

$$\dot{z}_{i'} = -b z_{i'} + x_{i'} y_{i'}. \tag{12}$$

Figure 9 shows $\langle \sigma \rangle$ between the original Lorenz network and its replica as a function of ε for all i. For $\varepsilon < 10$, the global dynamics represents the monotonous US behavior (not presented). The results in the diagram also unveil the nontrivial feature of transitions from partial to global synchronization in scale-free dynamical networks. The dependence of synchronization thresholds ε_c on the degree of nodes k is plotted in Fig. 6 as triangles.

IV. CONCLUSION

Most of the previous studies of GS have focused on two unidirectionally coupled nonidentical systems, which reveal a stable, refined, and smooth functional relation. In the present paper, the auxiliary-system method has been applied to detect the GS behavior in mutually coupled maps and scale-free networks of chaotic elements. We have demonstrated that coherence with such a level is realizable in both systems. Two types of dynamical behaviors, namely IPGS and IGGS, are detected near the synchronization thresholds. Furthermore, these intermittent behaviors are shown as the typical on-off intermittence with the typical exponent $-3/2$. The detailed analysis shows that the dynamical process toward synchronization represents the transitions from partial to global GS. With respect to the heterogeneously dynamical networks, paths to global synchronization reveal a cascading order highly depending on topological properties. Our results show that GS starts from some central node with a large number of degree, or hub, then distributes over the whole network by asynchronously grouping the nodes connecting to them.

It should be emphasized that the GS behavior detected in the network indicates the existence of a functional relationship between a node and its local mean field, rather than the explicit coherence between any two nodes. The PGS state in networks then defines the situation in which some nodes have been entrained (by local mean fields) while the others have not. Analogously, the GGS indicates that functional relations between the nodes and their local mean fields have been globally established. Actually, we have applied the nonlinear measurement, the interdependence [41], to detect the coherent relationship among the dynamics of nodes. When all nodes are entrained, we found several classes of correlation among them. First, the two connected nodes are weakly and asymmetrically dependent. Second, all nodes with $k = 1$ and connected to the same node are completely synchronized. Otherwise, any two unconnected nodes which do not

connect directly with the same node evolve almost independently.

It is important to point out that the PGS transition is observed for sparsely connected networks, especially the one with the tree structure, but is difficult to identify when the number of connections increases further (in our case $m \geq 3$). Although the transition scenario can be regarded as a specific feature in treelike heterogeneous networks, in nature there are many real systems belonging to this category, such as the brain functional network [42]. The paths to synchronization then provide us insight into the synchronization process in these systems. In brief, the topological hubs of the heterogeneous networks also play the essential role in the process of synchronization.

Very recently, Bag, Petrosyan, and Hu [3] studied the influence of various noises on the synchronization of the stochastic Kuramoto model. It is of interest to put the stochastic Kuramoto model or other models on SFN and to study the influence of various noises on the paths to synchronization of such models on SFN.

ACKNOWLEDGMENTS

This work was supported by the National Science Council of Taiwan under Grant Nos. NSC 96-2911-M001-003-MY3 and NSC 96-2112-M017-001-MY3 and National Center for Theoretical Sciences in Taiwan.

[1] A. S. Pikovsky, M. G. Rosenblum, and J. Kurths, *Synchronization: A Univeral Concept in Vonlinear Sciences* (Cambridge University Press, Cambridge, 2001); J. A. Acebrón *et al.*, Rev. Mod. Phys. **77**, 137 (2005).

[2] P. M. Gade and C.-K. Hu, Phys. Rev. E **60**, 4966 (1999); **73**, 036212 (2006).

[3] B. C. Bag, K. G. Petrosyan, and C.-K. Hu, Phys. Rev. E **76**, 056210 (2007).

[4] K. Otsuka, R. Kawai, S.-L. Hwong, J.-Y. Ko, and J.-L. Chern, Phys. Rev. Lett. **84**, 3049 (2000); K. Otsuka, T. Ohtomo, A. Yoshioka, and J.-Y. Ko, Chaos **12**, 678 (2002).

[5] J. Hassel, L. Grönberg, P. Helistö, and H. Seppä, Appl. Phys. Lett. **89**, 072503 (2006).

[6] I. Goychuk, J. Casado-Pascual, M. Morillo, J. Lehmann, and P. Hänggi, Phys. Rev. Lett. **97**, 210601 (2006).

[7] C. Schäfer, M. G. Rosenblum, J. Kurths, and H.-H. Abel, Nature (London) **392**, 239 (1998); C. Schäfer, M. G. Rosenblum, H.-H. Abel, and J. Kurths, Phys. Rev. E **60**, 857 (1999); M.-C. Wu and C.-K. Hu, *ibid.* **73**, 051917 (2006).

[8] S. Rajesh, S. Sinha, and S. Sinha, Phys. Rev. E **75**, 011906 (2007).

[9] R. E. Amritkar and G. Rangarajan, Phys. Rev. Lett. **96**, 258102 (2006).

[10] I. Z. Kiss, Q. Lv, and J. L. Hudson, Phys. Rev. E **71**, 035201(R) (2005).

[11] M.-C. Wu, M.-C. Huang, H.-C. Yu, and T. C. Chiang, Phys. Rev. E **73**, 016118 (2006); M.-C. Wu, Physica A **375**, 633 (2007).

[12] L. M. Pecora and T. L. Carroll, Phys. Rev. Lett. **64**, 821 (1990); K. Kaneko, *ibid.* **65**, 1391 (1990).

[13] A. Pikovsky, M. Zaks, M. Rosenblum, G. Osipov, and J. Kurths, Chaos **7**, 680 (1997); A. Pikovsky, G. Osipov, M. Rosenblum, M. Zaks, and J. Kurths, Phys. Rev. Lett. **79**, 47 (1997); B. Hu and Z. Liu, Phys. Rev. E **62**, 2114 (2000); M.-C. Ho, Y.-C. Hung, and I.-M. Jiang, Phys. Lett. A **324**, 450 (2004); H. Hong, H. Park, and M.-Y. Choi, Phys. Rev. E **70**, 045204(R) (2004).

[14] U. Parlitz, L. Junge, and L. Kocarev, Phys. Rev. Lett. **79**, 3158 (1997).

[15] M. G. Rosenblum, A. S. Pikovsky, and J. Kurths, Phys. Rev. Lett. **78**, 4193 (1997); S. Taherion and Y.-C. Lai, Phys. Rev. E **59**, R6247 (1999).

[16] H. U. Voss, Phys. Rev. E **61**, 5115 (2000); H. U. Voss, *ibid.* **64**, 039904(E) (2001); H. U. Voss, Phys. Rev. Lett. **87**, 014102 (2001).

[17] R. Femat and G. Solís-Perales, Phys. Rev. E **65**, 036226 (2002); M.-C. Ho, Y.-C. Hung, Z.-Y. Liua, and I.-M. Jiang, Phys. Lett. A **348**, 251 (2006).

[18] S. Boccaletti, L. M. Pecora, and A. Pelaez, Phys. Rev. E **63**, 066219 (2001); A. E. Hramov and A. A. Koronovskii, Chaos **14**, 603 (2004).

[19] S. H. Strogatz, Nature (London) **410**, 268 (2001); T. Nishikawa, A. E. Motter, Y.-C. Lai, and F. C. Hoppensteadt, Phys. Rev. Lett. **91**, 014101 (2003); A. E. Motter, M. A. Matias, J. Kurths, and E. Ott, Physica D **224**, vii (2006).

[20] P. M. Gade and C.-K. Hu, Phys. Rev. E **62**, 6409 (2000); M. Barahona and L. M. Pecora, Phys. Rev. Lett. **89**, 054101 (2002); H. Hong, M.-Y. Choi, and B.-J. Kim, Phys. Rev. E **65**, 026139 (2002); C.-G. Li and G.-R. Chen, *ibid.* **68**, 052901 (2003); H. Hong, B.-J. Kim, M.-Y. Choi, and H. Park, *ibid.* **69**, 067105 (2004).

[21] D. J. Watts and S. H. Strogatz, Nature (London) **393**, 440 (1998).

[22] R. Albert, H. Jeong, and A.-L. Barabási, Nature (London) **401**, 130 (1999); A.-L. Barabási and R. Albert, Science **286**, 509 (1999); R. Albert and A.-L. Barabási, Rev. Mod. Phys. **74**, 47 (2002).

[23] D.-S. Lee, Phys. Rev. E **72**, 026208 (2005); S.-H. He, H.-B. Huang, X. Zhang, Z.-X. Liu, D.-S. Xu, and C.-K. Shen, *ibid.* **74**, 057203 (2006).

[24] W.-X. Qin and G.-R. Chen, Physica D **197**, 375 (2004); B. Ao and Z.-G. Zheng, Europhys. Lett. **74**, 229 (2006).

[25] S. Jalan and R. E. Amritkar, Phys. Rev. Lett. **90**, 014101 (2003); S. Jalan, R. E. Amritkar, and C.-K. Hu, Phys. Rev. E **72**, 016211 (2005); R. E. Amritkar, S. Jalan, and C.-K. Hu, *ibid.* **72**, 016212 (2005); R. E. Amritkar and C.-K. Hu, Chaos **16**, 015117 (2006).

[26] S. Camazine, J. L. Deneubourg, N. R. Franks, J. Sneyd, G. Theraulaz, and E. Bonabeau, *Self-Organization in Biological Systems* (Princeton University Press, Princeton, NJ, 2001).

[27] R. Ferri, C. J. Stam, B. Lanuzza, F. I. Cosentino, M. Elia, S. A. Musumeci, and G. Pennisi, Clin. Neurophysiol. **115**, 1202

(2004); B. Percha, R. Dzakpasu, M. Żochowski, and J. Parent, Phys. Rev. E **72**, 031909 (2005).
[28] C.-Y. Yin, W.-X. Wang, G.-R. Chen, and B.-H. Wang, Phys. Rev. E **74**, 047102 (2006); P. G. Lind, J. A. C. Gallas, and H. J. Herrmann, *ibid.* **70**, 056207 (2004).
[29] H. D. I. Abarbanel, N. F. Rulkov, and M. M. Sushchik, Phys. Rev. E **53**, 4528 (1996).
[30] Z. Zheng, X. Wang, and M.-C. Cross, Phys. Rev. E **65**, 056211 (2002).
[31] S.-G. Guan, K. Li, and C.-H. Lai, Chaos **16**, 023107 (2006).
[32] M. Henon, Commun. Math. Phys. **50**, 69 (1976).
[33] M. de Sousa Vieira and A. J. Lichtenberg, Phys. Rev. E **56**, R3741 (1997); A. M. Batista and R. L. Viana, Phys. Lett. A **286**, 134 (2001); A. M. Batista, S. E. de S. Pinto, R. L. Viana, and S. R. Lopes, Phys. Rev. E **65**, 056209 (2002).
[34] C.-S. Zhou and C.-H. Lai, Phys. Rev. E **58**, 5188 (1998); C.-S. Zhou and C.-H. Lai, Physica D **135**, 1 (2000).
[35] D.-H. He, M. Zhan, and C.-H. Lai, Phys. Lett. A **326**, 349 (2004).
[36] G. L. Baker, J. A. Blackburn, and H. J. T. Smith, Phys. Rev. Lett. **81**, 554 (1998).
[37] A. E. Hramov and A. A. Koronovskii, Europhys. Lett. **70**, 169 (2005).
[38] Note that the local dynamics depends on the initial conditions sensitively. For a node, once the MCLE $\lambda_c > 0$ in one realization, $\langle \sigma_i \rangle$ would be larger than zero at the corresponding ε, even though the averaged MCLE $\langle \lambda_c \rangle$ among all realizations remains negative. Therefore, the averaged positive MCLE $\langle \lambda_c^+ \rangle$ is used to determine synchronization thresholds rather than the intuitive one $\langle \lambda_c \rangle$.
[39] A. Arenas, A. Díaz-Guilera, and C. J. Pérez-Vicente, Phys. Rev. Lett. **96**, 114102 (2006); J. Gómez-Gardeñes, Y. Moreno, and A. Arenas, *ibid.* **98**, 034101 (2007).
[40] E. N. Lorenz, J. Atmos. Sci. **20**, 130 (1963).
[41] M.-C. Ho and F.-C. Shin, Phys. Rev. E **67**, 056214 (2003).
[42] V. M. Eguíluz, D. R. Chialvo, G. A. Cecchi, M. Baliki, and A. V. Apkarian, Phys. Rev. Lett. **94**, 018102 (2005).